Multiphysics coupling between periodic gear mesh excitation and input/output fluctuating torques: Application to a roots vacuum pump

Pierre Garambois, Guillaume Donnard, Emmanuel Rigaud, Joël Perret-Liaudet

Multiphysics coupling between periodic gear mesh excitation and input/output fluctuating torques: application to a roots vacuum pump

Pierre Garambois[a,b], Guillaume Donnard[a,c], Emmanuel Rigaud[a,d], Joël Perret-Liaudet[a,e]

[a] *Laboratoire de Tribologie et Dynamique des Systèmes, UMR CNRS 5513*
Ecole Centrale de Lyon, member of Université de Lyon, 36 avenue Guy de Collongue 69134 Ecully Cedex, France
[b] *pierre.garambois@ec-lyon.fr*
[c] *guillaume.donnard@ec-lyon.fr*
[d] *emmanuel.rigaud@ec-lyon.fr*
[e] *joel.perret-liaudet@ec-lyon.fr*

Abstract

This paper presents the analysis of multiphysics coupling between periodic gear mesh excitation and upstream/downstream fluctuating loads using an iterative spectral methodology. This one is based on the resolution of the parametric equations of motion in the spectral domain. Its efficiency makes possible to treat both low and high frequency excitations for systems having a large number of degrees-of-freedom. The different excitation sources, the dynamic coupled equations of motion, the spectral methodology and the iterative resolution principle are described. The dynamic responses of a roots vacuum pump for which the spur gear high mesh frequency parametric excitation is coupled with a low fluidic drag torque frequency. The coupling between excitations generates a frequency enrichment of the dynamic response which is reflected on waterfall plots by emergence of numerous sidebands around harmonics of the mesh frequency.

Keywords: Vibrations, Gear Dynamics, Spectral Iterative Method, Parametric System, Power Transmission, Numerical Methods.

Nomenclature

$\mathbf{B}$	Modal basis composed of eigenvectors $\mathbf{V}_k$
$C(t)$	Torques on the shafts $(C_1(t) + C_2(t)$
$C_1(t)$	Torque on each lobe of shaft 1
$C_2(t)$	Torque on each lobe of shaft 2
$\mathbf{C}$	Viscous damping matrix
$\mathbf{e}(\theta)$	Vector describing the initial gap between the teeth at the angular position θ
$E(\omega)$	Dynamic Transmission Error (DTE)
$E^s(\omega)$	Fourrier Transform of $\Delta^s(t)$
$E^{(n)}(\omega)$	Dynamic Transmission Error (DTE) at step n
$\mathbf{f}$	Nodal coordinate vector of the only external force considered
$\mathbf{f}_S$	Static mesh force vector in the finite element model
$\mathbf{f}_{NL}$	Non-linear mesh force depending on $\mathbf{x}$ and θ
$\mathbf{f}_j$	Nodal coordinate vector of the external force j
f	Rotation frequency of the gear
$f_D(t)$	Dynamic mesh force in the time domain
f_m	Mesh frequency
f_{NL}	Scalar non-linear force acting in the plane of action
F	Static mesh load transmitted by the gear
$F_D(\omega)$	Dynamic mesh force in the spectral domain
$g(t)$	Centered fluctuation of the mesh stiffness
$G(\omega)$	Fourrier Transform of $g(t)$
$H_k(\omega)$	Frequency Response Function of the k mode
$\overline{k}$	Average mesh stiffness
$k(t)$	Fluctuating mesh stiffness
k_{sin}	Sinusoidal mesh stiffness
k_{sq}	Square mesh stiffness
$K(\omega)$	Fourrier Transform of $k(t)$
$\mathbf{K}_{AV}$	Global time-averaged stiffness matrix (considering the coupling between wheels)
$\mathbf{K}_{FE}$	Global stiffness matrix of the finite element model (except the coupling between wheels)

L	Number of external forces
$\mathbf{M}_{FE}$	Global mass matrix of the finite element model
n_E	Harmonic of the external excitation (multiple of ω_0)
n_M	Harmonic of the internal (meshing) excitation (multiple of ω_0)
N	Number of modes
$\mathbf{p}(\theta)$	Vector of the distributed loads along the contact line at the angular position θ
p_i	Load at the discretized contact point i
$\mathbf{q}$	Modal coordinate vector
q_k	Component of the modal coordinate vector $\mathbf{q}$ for the k mode
$Q_k(\omega)$	Fourrier Transform of q_k of the k mode
$\mathbf{r}$	Geometrical vector projected in the modal basis
r_k	Component of the geometrical vector projected in the modal basis $\mathbf{q}$ for the k mode
$\mathbf{R}$	Geometrical vector associated with the gear design
$\mathbf{S}(\theta)$	Compliance matrix of the teeth in contact at the angular position θ
$S(\omega)$	Weighted spectrum representing the STE in the spectral domain
$T(\omega)$	Scalar function representing the spatial and resonance sensibility to the mesh modes
$\mathbf{V}_k$	Eigenvectors of the k mode
$W(\omega)$	Weighted spectrum representing the external forces in the spectral domain
$\mathbf{x}$	N-degrees-of-freedom column vector
$\mathbf{x}_s$	Static equilibrium position
$X_j(\omega)$	Response of the degree-of-freedom j in the spectral domain
Z	Number of teeth pf the gear
$\Delta^s(\theta)$	Static Transmission Error (STE) at the angular position θ
ϵ	Stop criterion
$\gamma(t)$	Scalar temporal function representing the time-evolution of the only external force considered in the calculation
$\gamma_j(t)$	Scalar temporal function representing the time-evolution of the external force $\mathbf{f}_j$
$\boldsymbol{\phi}$	Projection of the nodal coordinate vector of the external force onto the modal basis
ω	Steady-state operating rotation speed
ω_k	Eigenfrequencies of the eigenvectors $\mathbf{V}_k$

ω_0	Fundamental frequency
ω_{ext}	External excitations frequency
ω_{int}	Internal excitations frequency
ω_{rep}	Response frequency
ϕ_k	Component of the nodal coordinate vector of the external force $\boldsymbol{\phi}$ projected onto the modal basis the for the k mode
ρ_k	Energy contribution of the k mode
θ	Angular position of the driving wheel
ζ_k	Modal damping of k mode
$\otimes$	Convolution product

1. Introduction and background

Gear power transmissions are responsible for upsetting vibroacoustic phenomena [1]. One of the main excitation sources of gearboxes is generated by the meshing process. It is usually assumed that static transmission error (STE) and gear mesh stiffness fluctuations are responsible of the noise radiated by the gearbox [2]. STE is defined as the difference between the actual position of the output toothed wheel and the position it would occupy if the gear drive were perfect [3]. Its characteristics depend on the instantaneous situations of the meshing tooth pairs resulting from tooth deflections and micro-level geometry (voluntary tooth profile modifications and manufacturing errors).

The calculation of STE of a gear transmission under the static mesh load F is well mastered [4, 5]. It is based on linear elasticity and the solving of the static contact equation between geared wheels (only considering the in-plane effects).
For each input angular position θ of the driving wheel, a kinematic analysis of the meshing process is used to determine the theoretical contact line over the teeth (potential position of the contact on the teeth in the plane of action). These lines are discretized, in order to introduce a compliance matrix $\mathbf{S}(\theta)$ built from a modeling of toothed wheels in a prior calculation, taking into account all physical phenomena that contribute to the deflections. The thiner the wheel body, the higher its influence and the interaction between the teeth in contact [4, 5]. The Hertz deformation is also taken into account in the matrix $\mathbf{S}(\theta)$. The tooth corrections and the manufacturing errors [6] are introduced through a vector $\mathbf{e}(\theta)$ that describes the initial gap between the teeth. This vector $\mathbf{e}(\theta)$ also takes into account the parallelism errors that come from the elasto-static deformation of the whole gearbox. For each position θ, the resolution of the contact equations allows the evaluation of the STE quoted $\Delta^s(\theta)$, and to the vector of the distributed loads $\mathbf{p}(\theta)$ describing the load distribution along the contact lines. The corresponding system of equations is:

$$\begin{cases} \mathbf{S}(\theta).\mathbf{p}(\theta) = \Delta^s(\theta).\mathbf{1} - \mathbf{e}(\theta) \\ \mathbf{1}^T.\mathbf{p}(\theta) = F \end{cases} \tag{1}$$

under the constraints:

$$\begin{cases} \mathbf{S}(\theta).\mathbf{p}(\theta) + \Delta^s(\theta).\mathbf{1} \geqslant \mathbf{e}(\theta) \\ p_i \leqslant 0 \end{cases} \tag{2}$$

For a constant speed, STE is a θ-periodic function and its main spectral components are associated with harmonics of the mesh frequency ($f_m = Z.f$, with f the rotation frequency of the gear and Z the number of teeth).
STE is also responsible of fluctuation of the mesh stiffness $k(t)$ which generates a periodic parametric internal excitation. For each position θ, it corresponds to the derivate of the force with respect to the STE, as follows:

$$k(\theta) = \frac{\partial F}{\partial \Delta^s(\theta)} \tag{3}$$

Practically, it is estimated by numerical derivation rule. The excitations are described in figure 1.

Under steady-state operating conditions, STE and mesh stiffness fluctuations are periodic and generate dynamic mesh forces which are transmitted to the housing through wheel bodies, shafts and bearings. Housing vibratory state is directly related to the whining noise radiated from the gearbox.

The sensitivity of the STE to the micro-level geometry has been widely studied [6, 7, 8, 9, 10, 11, 12, 13, 14, 15, 16], as well as the influence of the wheel body deflection and the coupling be-

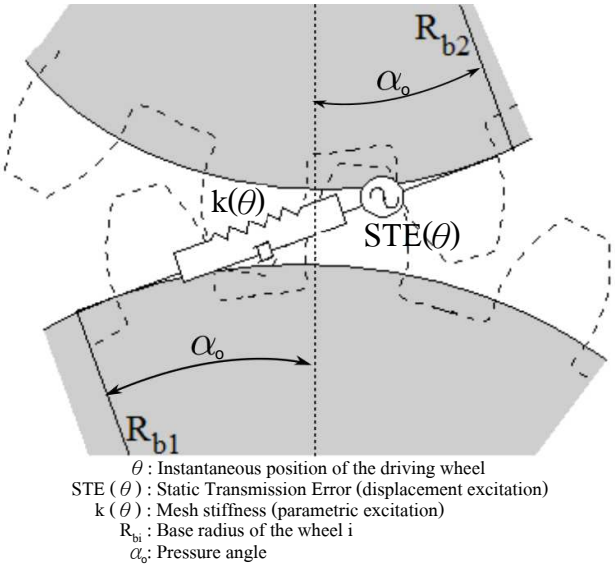

Figure 1: *Excitation sources generated by the meshing process [4]*

tween the different teeth in the meshing process [4, 5]. Many authors have proposed methodologies to define a set of micro-level teeth corrections leading to minimizing the STE fluctuation and the corresponding emitted whining noise [6, 8, 11, 17]. The influence of micro-level corrections on the load distribution, the gear stress and the gear wear has also been studied [14, 13].
The mesh stiffness is usually deduced from STE estimation [4, 5, 18, 19]. Welbourn has suggested an average value of 13.9 $N.\mu m^{-1}$ per tooth width millimeter for standard spur gears [2].

Many different models have been proposed to study the dynamic behavior of gear systems [20]. They may be distinguished according to the mesh coupling definition:

- Linear models with constant parameters have been implemented [21, 22]. In these cases, an average value of mesh stiffness is introduced and STE corresponds to a displacement-type excitation. A large review is available in the literature [20].
- Linear models with fluctuating parameters have also been implemented [23, 24, 25]. In these cases, a time fluctuation of the mesh stiffness is taken into account.
- Non-linear models with time-invariant average stiffness have been studied [26, 27, 28, 29].
- Non-linear models including backlash with fluctuating mesh stiffness have also been widely studied. Some models only focus on the effect of internal excitations [30, 31, 32, 33]. In the case of external fluctuating forces, both case of rattle noise [34, 35, 36, 37, 38, 39] and hammering noise [40, 41, 42, 43, 44] were studied in the literature.
- The parametric excitation associated with its fluctuation may lead to instabilities and parametric resonances [45, 46] of the dynamic response.

In some specific cases, an analytical or semi-analytical solution may be obtained for the linear parametric modeling of the equation of motion [47]. Nevertheless, this analytical approach is possible only for very simple gear systems. For real geared systems whose discretized model presents a large number of degrees-of-freedom, computing time may also become a problem. The excitation sources

are characterized by various frequency components, so that the time discretization methods generally fail to solve the system of parametric equations of motion, since a short time step is needed, as well as a simulation during a long time range. Consequently, an alternative method has been proposed [25, 48, 19]. This iterative spectral method is based on the solving of the linear parametric equations of motion in the spectral domain and leads to reduce the computation time. It has been used to predict and analyze the dynamic response and whining noise for mono [18, 49, 48, 19] and multi-gear systems [50]. The variability of the dynamic response generated by the micro-level manufacturing errors has also been studied [51, 52], as well as the dynamic response induced by an external random excitation with gyroscopic terms [53, 54].

The present work aims to extend the spectral iterative method in order to take into account the couplings between the mesh stiffness fluctuations and the other excitation sources of the mechanical system. Indeed, this last is often submitted to torque variations of upstream and/or downstream devices in addition to the internal excitation generated by the meshing process. Depending on the object studied, this coupling may associate both high and low frequencies. The first part (sections 2 and 3) describes the parametric equations of motion in the physical and modal basis, taking account of excitation sources generated by upstream/downstream devices, and the resolution method. The second part (sections 4 and 5) presents the advantage of the method in term of computational time and the physical phenomena at stake in the coupling. The third part (section 6) presents to the analysis of the dynamic responses for a root vacuum pump designed with a 1:1 gear ratio and submitted to a fluid narrow band excitation. The corresponding mesh stiffness fluctuation is characterized by high frequency components ($f_m = Z.f$, with f the rotation frequency of the gear and Z the number of teeth: $Z = 76$) and the pumping excitation is characterized by low frequency components ($f_p = 4.f$, due to the figure-eight lobes mounted on the counter-rotating shafts of the pump).

2. Parametric equation of motion of the discretized model

The dynamic response of a gear transmission system, in the case of the whining noise, may be described in the frequency modal domain. Most of the modeling are based on a finite element model. In this context, it is necessary to introduce coupling elements which represent the meshing action between the toothed wheel.

2.1. Linearization of the mesh force and matrix equation in the physical basis

Consider a gear system discretized with a N-degrees-of-freedom finite element model, the static equilibrium is written as follows:

$$\mathbf{K}_{FE}\mathbf{x} + \mathbf{f}_{NL}(\mathbf{x}, \theta) = \mathbf{f}_S \tag{4}$$

with $\mathbf{x}$ the N-degrees-of-freedom column vector, $\mathbf{K}_{FE}$ the global stiffness matrix (except for the coupling between wheels), $\mathbf{f}_S$ representing the static mesh force vector corresponding to the transmitted force F (see equation 1), $\mathbf{f}_{NL}(\mathbf{x}, \theta)$ the non-linear mesh force that depends on $\mathbf{x}$ and θ the rotational angle of the input wheel. This meshing force is responsible for the STE and the mesh stiffness time fluctuation.

The interaction between teeth depends on the rigid body displacement of the wheels. It can be

related to $\mathbf{x}$ via a geometrical vector $\mathbf{R}$ associated with the gear design. This N-coordinates vector has 12 non-null values which couples the 6 degrees-of-freedom of the pinion center to the 6 degrees-of-freedom of the driving wheel center. In fact, the STE $\Delta^s(t)$ can be written as the following scalar product:

$$\Delta^s(t) = \mathbf{R}^T \mathbf{x}_s(t) \tag{5}$$

with $\mathbf{x}_s(t)$ the static equilibrium position. We may generalize this notion by introducing the Dynamic Transmission Error (DTE) $\Delta(t)$:

$$\Delta(t) = \mathbf{R}^T \mathbf{x}(t) \tag{6}$$

The N-coordinates non-linear mesh force vector $\mathbf{f}_{NL}$ is related to the scalar transmitted force f_{NL} acting in the plan of action through the same geometrical vector:

$$\mathbf{f}_{NL}(\mathbf{x}, \theta) = \mathbf{R} f_{NL}(\mathbf{R}^T \mathbf{x}, \theta) = \mathbf{R} f_{NL}(\Delta, \theta) \tag{7}$$

The meshing force is linearized in order to be easily introduced in the finite element model with the following rule:

$$\mathbf{f}_{NL}(\mathbf{x}, \theta) \approx \mathbf{f}_{NL}(\mathbf{x}_s, \theta) + \Big(\frac{\partial \mathbf{f}_{NL}}{\partial x}\Big)_{\mathbf{x}_s} (\mathbf{x} - \mathbf{x}_s) \tag{8}$$

From equation 5, 6 and 7, one obtains:

$$\mathbf{f}_{NL}(\mathbf{x}, \theta) \approx \mathbf{R} f_{NL}(\Delta^s, \theta) + \mathbf{R}\mathbf{R}^T \Big(\frac{\partial f_{NL}}{\partial \Delta}\Big)_{\Delta^s} (\mathbf{x} - \mathbf{x}_s) \tag{9}$$

By condensing the transmitted force vector $\mathbf{f}_S$ to the line of action, and with a judicious choice of coordinate $\mathbf{x}_s$, the static force problem can be replace by:

$$\mathbf{f}_S = \mathbf{R} f_{NL}(\Delta^s, \theta) \tag{10}$$

with

$$\mathbf{K}_{FE} \mathbf{x}_s = 0 \tag{11}$$

In equation 9, the derivative represents the mesh stiffness introduced in section 1):

$$k(\theta) = \Big(\frac{\partial f_{NL}}{\partial \Delta}\Big)_{(\Delta^s)} \tag{12}$$

At first order, θ can be replaced by a time-dependent function. For steady-state operating conditions ω and a periodic rotation, θ can be simply expressed as follows:

$$\theta = \omega t \tag{13}$$

By considering equations 4, 9, 10, 12 and 13, the standard dynamic matrix equation of motion for whining noise can now be written as follows:

$$\mathbf{M}_{FE} \ddot{\mathbf{x}} + \mathbf{C} \dot{\mathbf{x}} + \mathbf{K}_{FE} \mathbf{x} + k(t) \mathbf{R}\mathbf{R}^T \mathbf{x} = k(t) \mathbf{R}\mathbf{R}^T \mathbf{x}_s(t) \tag{14}$$

with $\mathbf{M}_{FE}$ the mass matrix of the finite element model, $\mathbf{C}$ a viscous damping matrix defined a posteriori through equivalent modal damping coefficients.
$k(t)$ is periodic (see section 1) and can be written as follows:

$$k(t) = \overline{k} + g(t) \tag{15}$$

with $\overline{k}$ the average mesh stiffness and $g(t)$ the centered fluctuation of the mesh stiffness. $\mathbf{K}_{AV}$ matrix is introduced. It corresponds to the global time-averaged stiffness matrix:

$$\mathbf{K}_{AV} = \mathbf{K}_{FE} + \overline{k} \mathbf{R}\mathbf{R}^T \tag{16}$$

The matrix equation can be summarized in the following form:

$$\mathbf{M}_{FE} \ddot{\mathbf{x}} + \mathbf{C} \dot{\mathbf{x}} + \mathbf{K}_{AV} \mathbf{x} + g(t) \mathbf{R}\mathbf{R}^T \mathbf{x} = k(t) \mathbf{R} \Delta^s(t) \tag{17}$$

2.2. Introduction of the additional input/output torques

As mentioned in the introduction, the aim of this paper is to study the case of a gear transmission submitted to input and output external forces. Equation 17 then becomes:

$$\mathbf{M}_{FE}\ddot{\mathbf{x}} + \mathbf{C}\dot{\mathbf{x}} + \mathbf{K}_{AV}\mathbf{x} + g(t)\mathbf{R}\mathbf{R}^T\mathbf{x} = k(t)\mathbf{R}\Delta^s(t) + \sum_{j=1}^{L}\gamma_j(t)\mathbf{f}_j \tag{18}$$

with $\gamma_j(t)$ a scalar temporal function and $\mathbf{f}_j$ the nodal coordinate vector of the external force j. The system being linear, we consider in the rest of the paper, without loss of generality, a single force $\gamma(t)\mathbf{f}$.

2.3. Modal equation

The solution is projected onto the modal basis determined from the average characteristic $\mathbf{M}_{FE}$ and $\mathbf{K}_{AV}$ of the system. This modal basis is computed with the matrices $\mathbf{M}_{FE}$ and $\mathbf{K}_{AV}$. It leads to the L-vibrational eigenfrequencies ω_k and eigenvectors $\mathbf{V}_k$:

$$\mathbf{B} = \left[\mathbf{V}_k\right],\ \omega_k \tag{19}$$

normalized regarding the mass matrix:

$$\mathbf{B}^{(-1)}\mathbf{M}_{FE}\mathbf{B} = \mathbf{I} \tag{20}$$

The modal coordinate vector $\mathbf{q}$ is defined as follows:

$$\mathbf{x} = \mathbf{B}\mathbf{q} \tag{21}$$

The equation 18 can then be written as follows:

$$\mathbf{B}^{-1}\mathbf{M}_{FE}\mathbf{B}\ddot{\mathbf{q}} + \mathbf{B}^{-1}\mathbf{C}\mathbf{B}\dot{\mathbf{q}} + \mathbf{B}^{-1}\mathbf{K}_{AV}\mathbf{B}\mathbf{q} + g(t)\mathbf{B}^{-1}\mathbf{R}\mathbf{R}^T\mathbf{B}\mathbf{q} = k(t)\mathbf{B}^{-1}\mathbf{R}\Delta^s(t) + \gamma(t)\mathbf{B}^{-1}\mathbf{f} \tag{22}$$

The orthogonality properties of the eigenmodes lead to the following form:

$$\mathbf{diag}[1]\ddot{\mathbf{q}} + \mathbf{diag}[2\zeta_k\omega_k]\dot{\mathbf{q}} + \mathbf{diag}[\omega_k^2]\mathbf{q} + g(t)\mathbf{r}\mathbf{r}^T\mathbf{q} = k(t)\mathbf{r}\Delta^s(t) + \gamma(t)\boldsymbol{\phi} \tag{23}$$

with ζ_k the modal damping of mode k, $\mathbf{r} = \mathbf{B}^{-1}\mathbf{R}$ the geometrical vector projected in the modal basis, and $\boldsymbol{\phi} = \mathbf{B}^{-1}\mathbf{f}$ the projection of the nodal coordinate vector of the external force onto the modal basis. Notice that this equation remain coupled by the parametric term of the mesh stiffness leading to the N coupled modal equations:

$$\ddot{q}_k + 2\zeta_k\omega_k\dot{q}_k + \omega_k^2 q_k + g(t)r_k\sum_{l=1}^{N} r_l q_l = k(t)r_k\Delta^s(t) + \phi_k\gamma(t)\,,\quad k = 1..N \tag{24}$$

3. Projection onto the spectral domain and resolution

3.1. Equations in the spectral domain

The first principle of the spectral method is to solve the coupled equations 24 in the spectral domain, keeping only the steady-state response or forced response of the system. The free response is either a decreasing exponential (asymptotic stability) or an increasing exponential in the case

of parametric instabilities [48]. We assume the asymptotic stability of the system which can be done by a sufficient damping level to prevent parametric instabilities. The Fourier transform of the coupled equations 24 leads to:

$$H_k^{-1}(\omega)Q_k(\omega) + G(\omega)r_k \otimes \sum_{l=1}^{N} r_l Q_l(\omega) = K(\omega) \otimes r_k E^s(\omega) + \phi_k \Gamma(\omega) \tag{25}$$

or:

$$Q_k(\omega) + H_k(\omega)G(\omega)r_k \otimes \sum_{l=1}^{N} r_l Q_l(\omega) = H_k(\omega)K(\omega) \otimes r_k E^s(\omega) + H_k(\omega)\phi_k \Gamma(\omega) \tag{26}$$

with:

$$H_k(\omega) = \frac{1}{\omega_k^2 - \omega^2 + 2i\zeta_k\omega_k\omega} \tag{27}$$

the Frequency Response Function of the k mode, and $Q_k(\omega)$, $G(\omega)$, $K(\omega)$ and $E^s(\omega)$ respectively the Fourier transform of $q_k(t)$, $g(t)$, $k(t)$ and $\Delta^s(t)$, and finally $\otimes$ the convolution product.

The second principle of the method is to condense the N coupled equations on the line of action in order to explicit the Dynamic Transmission Error $E(\omega)$. The coupled equations system 26 is then turned into only one equation:

$$\begin{aligned}\sum_{k=1}^{N} r_k Q_k(\omega) + \sum_{k=1}^{N} r_k H_k(\omega)G(\omega)r_k \otimes \sum_{l=1}^{N} r_l Q_l(\omega) = \sum_{k=1}^{N} r_k H_k(\omega)K(\omega) \otimes r_k E^s(\omega) + \\ \sum_{k=1}^{N} r_k H_k(\omega)\phi_k \Gamma(\omega)\end{aligned} \tag{28}$$

The dynamic transmission error is defined in the spectral domain as follows:

$$E(\omega) = \sum_{l=1}^{N} r_l Q_l(\omega) \tag{29}$$

Equation 28 becomes:

$$E(\omega) + \sum_{k=1}^{N} r_k H_k(\omega)G(\omega)r_k \otimes E(\omega) = \sum_{k=1}^{N} r_k H_k(\omega)K(\omega) \otimes r_k E^s(\omega) + \sum_{k=1}^{N} r_k H_k(\omega)\phi_k \Gamma(\omega) \tag{30}$$

For the sake of simplicity, the following scalar function is introduced:

$$T(\omega) = \sum_{k=1}^{N} r_k^2 H_k(\omega) \tag{31}$$

It represents the frequency sensibility of the system regarding the meshing actions.
We also introduce:

$$W(\omega) = \sum_{k=1}^{N} r_k H_k(\omega)\phi_k \Gamma(\omega) \tag{32}$$

$$S(\omega) = \sum_{k=1}^{N} r_k^2 H_k(\omega)K(\omega) \otimes E^s(\omega) = T(\omega)K(\omega) \otimes E^s(\omega) \tag{33}$$

Finally the following scalar equation is obtained:

$$E(\omega) + T(\omega)\big[G \otimes E\big](\omega) = S(\omega) + W(\omega) \tag{34}$$

3.2. Principle of resolution

The third principle of the spectral iterative method is to iterate according to the following schema:

$$E^{(n+1)}(\omega) = S(\omega) + W(\omega) - T(\omega)\big[G \otimes E^{(n)}\big](\omega) \tag{35}$$

with the following initial condition:

$$E^{(1)}(\omega) = S(\omega) + W(\omega) \tag{36}$$

The stop criterion is based on the relative error between two iterations:

$$\epsilon = \frac{E^{(n+1)}(\omega) - E^{(n)}(\omega)}{E^{(n+1)}(\omega)} \tag{37}$$

which is compared to a sufficiently small value previously imposed. It appeared that using this criterion was always sufficient in the numerical simulations. Then, the iterative spectral method allows to compute directly the DTE .

3.3. Dynamic mesh force and nodal responses

In the time-dependent domain, the dynamic mesh force (including the mean force) associated with $f_D(t)$ is written as follows:

$$f_D(t) = k(t)\mathbf{R}^T\mathbf{x}(t) \tag{38}$$

In the spectral domain:

$$F_D(\omega) = \big[K \otimes E\big](\omega)\big](\omega) \tag{39}$$

This data provides a good insight of the spectral content and the dynamic response amplitude. They are chosen as the main data studied in the next part.
The Fourier transform $Q_k(\omega)$ of the modal coordinate vector $q_k(t)$ is deduced from equations 26 and 29:

$$Q_k(\omega) = H_k(\omega)\Big[r_k\big[K \otimes E^s - G \otimes E\big](\omega) + \phi_k\Gamma(\omega)\Big] \tag{40}$$

Finally, the response of any degree of freedom $X_j(\omega)$ of the discretized system is simply obtained, going back to the physical basis (see equation 21):

$$X_j(\omega) = \sum_{k=1}^{N} V_{jk}H_k(\omega)\Big[r_k\big(K \otimes E^s - G \otimes E\big)(\omega) + \phi_k\Gamma(\omega)\Big] \tag{41}$$

4. Computational time

The spectral iterative method developed in the last sections 2 and 3 is based on few principles that enable a fast computation:

- the dynamic response is projected onto the modal basis of the discretized system (section 2.3),
- the N equations of the system are condensed into a single equation representing the dynamic transmission error (section 3.1),
- the parametric equations are solved in the spectral domain using an iterative schema (sections 3.1 and 3.2).

These principles allow a substantial gain of computational time compared to a standard time integration, especially when a highly discretized mechanical system couples both low and high frequency excitations.

The applications were made using Matlab and C++ on a classical laptop equipped with an Intel Core i7-5500U processor (2.40 GHz) and a RAM memory of 16 Go. For example, in the case of a projection on $N = 650$ modes, a high frequency mesh stiffness composed of 5 components and a low frequency external excitation composed of 10 components, the computation of the dynamic response under steady-state conditions for one single operating frequency takes around 0.2 second instead of few tens of seconds with a time integration.

5. Physical phenomena

Before dealing with the application, we describe in the following section the main characteristics of the response.

5.1. Frequency characteristics of the response

The multi frequency nature of the steady-state response induced by purely harmonic external excitations is a dominant feature of the periodic parametric system. This behavior can be seen in the iterative equation 35 through the convolution product between the mesh stiffness and the DTE response at the previous step. Assuming the internal excitation frequency ω_{int} (related to the mesh stiffness fluctuation) and the external excitation frequency ω_{ext} (applied on the kinematic chain), the spectral content of the response frequency ω_{rep} (generated by the external excitation) is composed of frequency components equal to:

$$\omega_{rep} = |p\,\omega_{int} \text{ +/- } \omega_{ext}| \text{ with } p \in \mathbb{N} \tag{42}$$

The fundamental frequency is often related to the shaft frequency, typically ω_0.
The fundamental frequency of the internal excitation is the mesh frequency, and can be written as:

$$\omega_{int} = n_M\,\omega_0 \tag{43}$$

with n_M typically of the order of the number of teeth.
The fundamental frequency of the external excitation may be written as follows:

$$\omega_{ext} = n_E\,\omega_0 \tag{44}$$

Depending on the input/output systems, ω_{ext} may be of the same order, lower or higher than ω_{int}.

- Case 1: $n_E = 0$, $\omega_{rep} = p\,n_M\,\omega_0$ with $p \in \mathbb{N}$. In this case, there is no fluctuation of the external excitation. The response components are the harmonics of the internal excitation frequency (see figure 2a).

- Case 2: $n_E = n_M$, $\omega_{rep} = p\,n_M\,\omega_0$ with $p \in \mathbb{N}$. In this case, the internal and external excitations have the same frequency. The response components are the harmonics of the internal excitation frequency (see figure 2b).

- Case 3: $n_E < n_M$, $\omega_{rep} = |p\, n_M \text{ +/- } n_E|\, \omega_0$ with $p \in \mathbb{N}$. In this case, the internal excitation is characterized by higher frequency than the external excitation. The response is characterized by a low frequency component corresponding to the external excitation and high frequency components corresponding to the coupling between the external excitation and the internal mesh stiffness (see figure 2c).
- Case 4: $n_M < n_E$, $\omega_{rep} = |p\, n_M \text{ +/- } n_E|\, \omega_0$ with $p \in \mathbb{N}$. In this case, the internal excitation is characterized by lower frequency than the external excitation. The response is characterized by a high frequency component corresponding to the external excitation and high frequency components corresponding to the coupling between the external excitation and the internal mesh stiffness (see figure 2d).

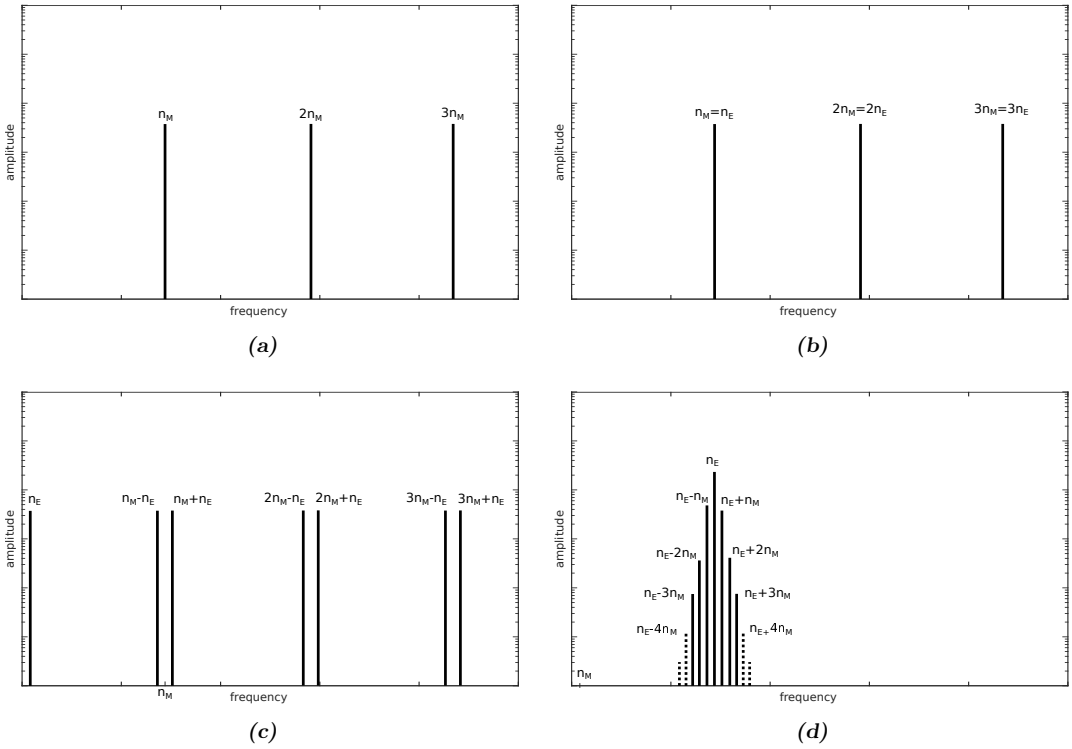

Figure 2: *Coupling phenomena between the external excitations (components n_E) and the internal mesh stiffness fluctuations (components n_M) in the DTE spectrum response (indexes corresponding to the harmonic multiple of the fundamental frequency ω_0). (a) Case 1: $n_E = 0$. (b) Case 2: $n_E = n_M$. (c) Case 3: $n_E < n_M$. (d) Case 4: $n_M < n_E$.*

This multi-frequency response is the result of the coupling phenomena. The amplitude of these components depend on the modal properties of the gear transmission. They are described in the following section.

5.2. Spatial and temporal filter

In the iterative scheme 35, the scalar function $T(\omega)$ (see equation 31) introduces the spatial and frequency sensitivity. Observing equation 31, the frequency filter is associated to the modal fre-

quency response $H_k(\omega)$ of each mode and the $r_k = \mathbf{B}_k^{-1}\mathbf{R}$ terms represent the spatial sensitivity localized at the meshing.

The modal discrimination regarding this sensitivity can be obtained by comparing all the static terms:

$$r_k^2 H_k(0) = \frac{r_k^2}{\omega_k^2} \tag{45}$$

In fact, these terms represent the energy contribution of each mode k [55]. We normalize these energy contributions of each mode k by introducing ρ_k as follows:

$$\rho_k = \frac{r_k^2}{\omega_k^2} \frac{1}{\sum_{k=1}^{N} \frac{r_k^2}{\omega_k^2}} \tag{46}$$

In such a way:

$$\sum_{k=1}^{N} \rho_k = 1 \tag{47}$$

The modes which have the highest energy rate ρ_k are called the mesh modes and are the most critical regarding the meshing process excitations.

Considering the multi-frequency nature of the system response (see equation 42), the operating conditions that may lead to parametric resonances are characterized by:

$$|p\,\omega_{int} \text{ +/- } \omega_{ext}| \approx \omega_k \text{ with } p \in \mathbb{N} \tag{48}$$

6. Application to a roots vacuum pump

This section presents the analysis of the dynamic response of a mechanical geared system taking account the coupling between the internal fluctuating mesh stiffness and the external excitations. It corresponds to a roots vacuum pump for which the spur gear mesh is associated with a high frequency parametric excitation and the pumping process is associated with a low frequency excitation.

6.1. Roots vacuum pump

The kinematic chain of the roots vacuum pump is designed with an asynchronous electric motor which drives two counter-rotative shafts using a reverse spur gear ($Z_1 = Z_2 = 76$). The characteristics of the gear are presented in table 1. Each shaft is supported by two rolling element bearings. Pumping is carried out using 6 figure-eight lobes mounted on each shaft and separated from each other and from the stator by narrow gap.

6.2. Kinematic chain modeling

The kinematic chain is modeled using the finite element method (see figure 3). Shafts are modeled using beam elements. Motor, gear wheels and lobes are modeled using concentrated mass elements and rotary inertias. Elastic coupling between toothed wheels is modeled using a symmetrical 12x12 stiffness matrix which couples the 6 degrees-of-freedom of the driven wheel with the 6 degrees-of-freedom of the driving wheel. Rolling element bearings are modeled using one axial and two radial

	Wheel 1 & 2
Number of teeth	76
Module (mm)	0.5
Pressure angle (degrees)	20
Facewidth (mm)	8
Helix angle (degrees)	0
Center distance (mm)	38
Average mesh stiffness $\overline{k}$ (N/μm)	307
Engine Torque (N.m)	10

Table 1: *Roots vacuum pump: characteristics of the spur gear (gear ratio 1:1)*

stiffnesses. The elastic model of kinematic chain has 130 elements, 110 nodes and 650 degrees-of-freedom.

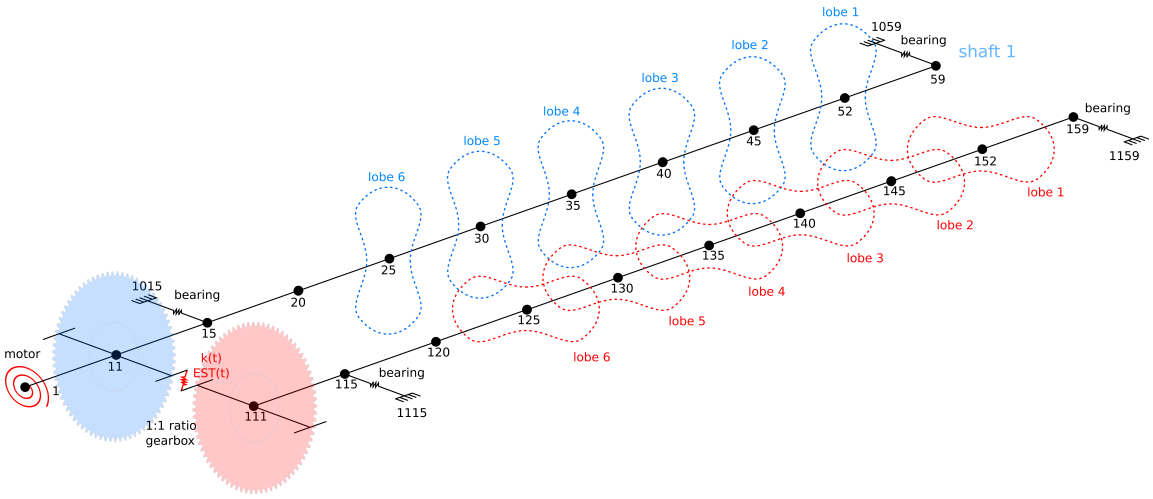

Figure 3: *Pump case: finite element model with components and lobe numbers*

6.3. Excitations sources

The coupling is illustrated using two different mesh stiffness cases $k(t)$ (see equation 15), in order to illustrate the richness of the spectral content.
The first one k_{sin} corresponds to a harmonic mesh stiffness fluctuation (with one spectral component at the mesh frequency f_m).

$$k_{sin}(t) = \overline{k}\left[1 + 0.2\, sin(2\pi f_m t)\right] \tag{49}$$

The second one k_{sq} corresponds to a square mesh stiffness fluctuation (with a theoretically infinite number of spectral components corresponding to odd harmonics of the mesh frequency).

$$\begin{aligned} k_{sq}(t) &= \overline{k}\left[1 + \frac{2\sqrt{2}}{5\pi}\sum_{l=0}^{\infty}\frac{sin((2l+1)2\pi f_m t)}{(2l+1)}\right] \\ &= \overline{k}\left[1 + \frac{2\sqrt{2}}{5\pi}\left[sin(\omega_m t) + \frac{1}{3}sin(3\omega_m t) + \frac{1}{5}sin(5\omega_m t) + \frac{1}{7}sin(7\omega_m t) + ...\right]\right] \end{aligned} \tag{50}$$

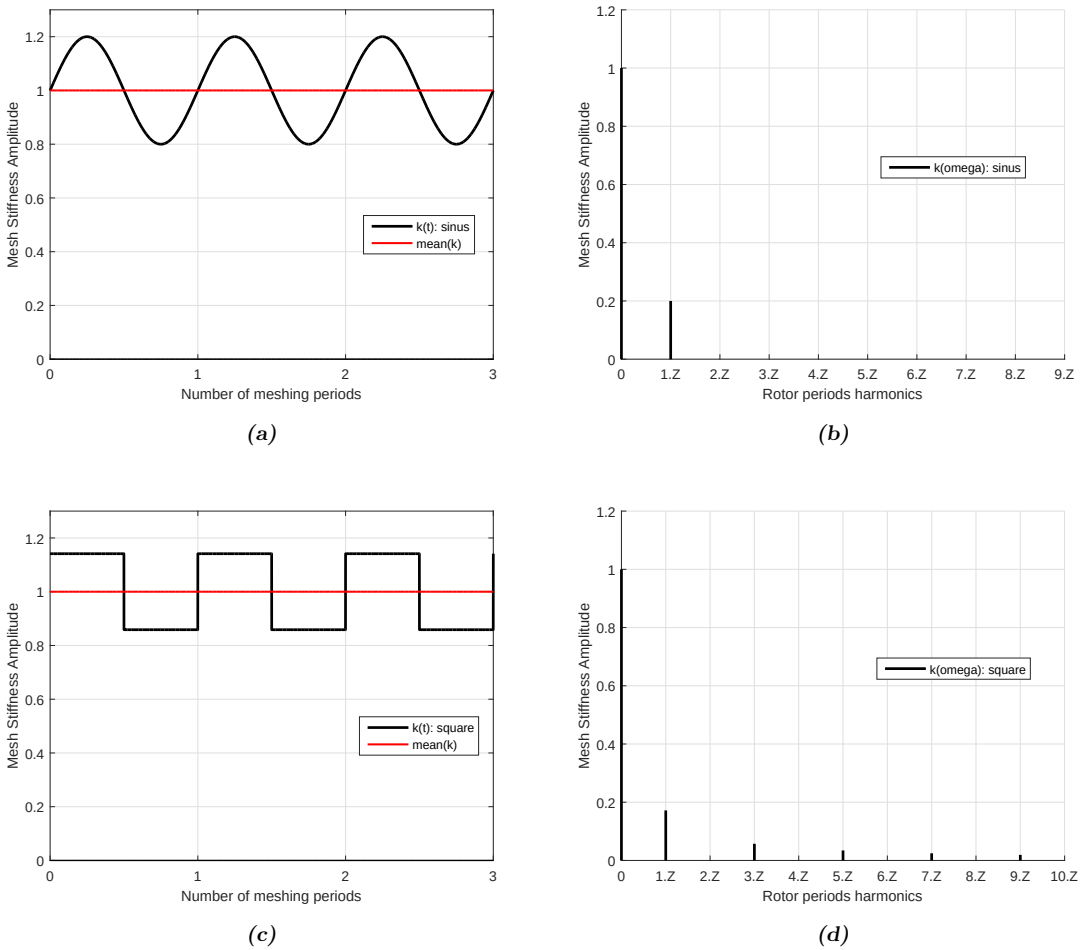

Figure 4: *Sinusoidal and square mesh stiffnesses time evolution and amplitude spectrum. (a) Sinusoidal mesh stiffness evolution $k_{sin}(t)$. (b) Sinusoidal mesh stiffness amplitude spectrum $k_{sin}(\omega)$. (c) Square mesh stiffness evolution $k_{sq}(t)$. (d) Square mesh stiffness amplitude spectrum $k_{sq}(\omega)$.*

Both k_{sin} and k_{sq} have a standard deviation corresponding to 14% of the mean value.

Besides the mesh stiffness fluctuations, two excitation sources are considered in addition to the mesh stiffness fluctuation. The first one corresponds to the static transmission error STE (see section 1) of the gear pair. It is a displacement type excitation which period is the meshing period. Considering that the fundamental frequency h1 is the motor frequency, its spectrum is composed of harmonics multiple of $Z = 76$ (h0, h76, h152, h228, h304 and h380). Figures 5a/b display the time evolution and the spectral content of STE.

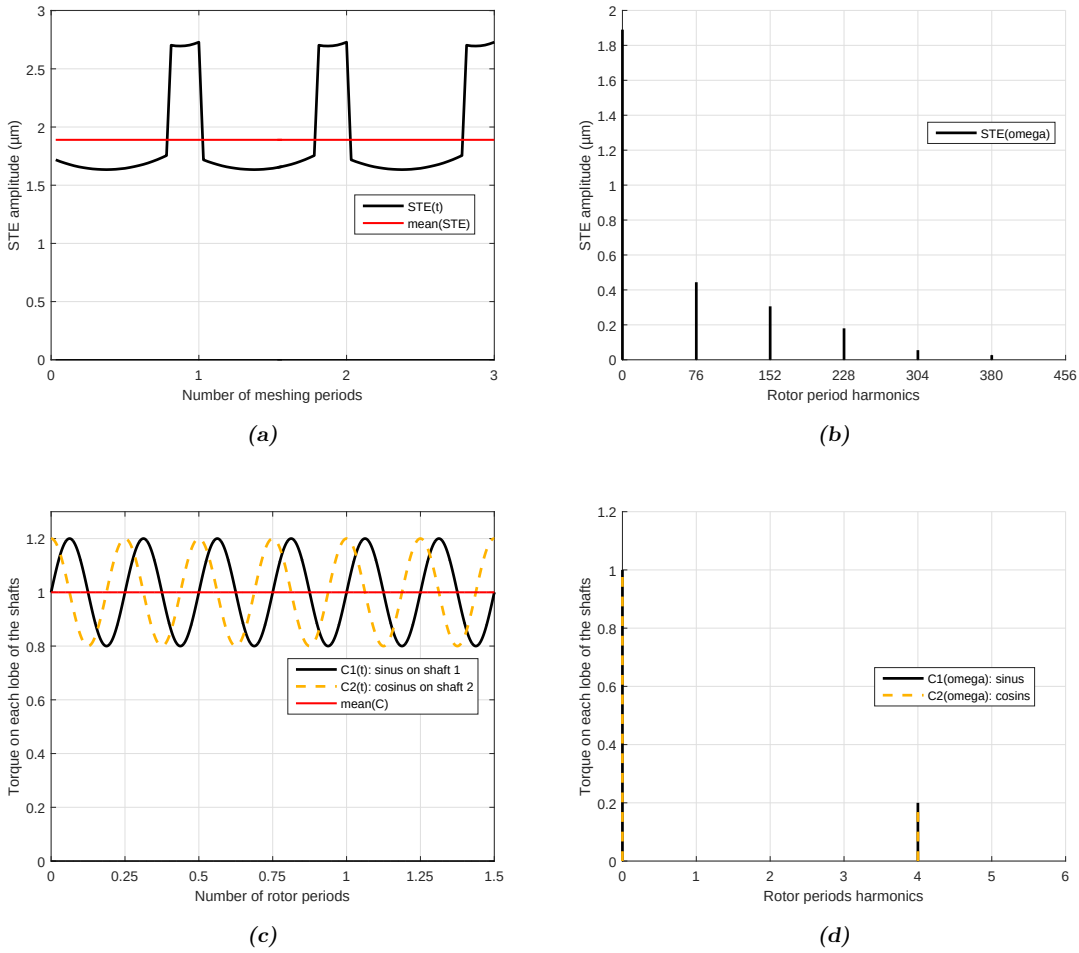

Figure 5: *Excitations applied on the root vacuum pump kinematic chain. (a) Static Transmission Error time evolution $STE(t)$. (b) Static Transmission Error spectral content $STE(\omega)$. (c) Time evolution of torques $C_1(t)$ (sinus) and $C_2(t)$ (cosinus) applied on shafts 1/2. (d) Spectral content of torques $C_1(\omega)$ (sinus) and $C_2(\omega)$ (cosinus) applied on shafts 1/2.*

The second excitation corresponds to fluidic drag torques applied to the shafts due to the pumping process. A sinusoidal excitation with the same amplitude and fundamental frequency h4 is assumed for each lobe. The fluctuation corresponds to 20% of the drag torque mean value of each lobe, the mean value of each lobe being equal to $\frac{1}{12}^{\text{th}}$h of the motor torque (10 N.m). A phase shift equal to $\frac{\pi}{2}$ is introduced between lobes mounted on shaft 1 and lobes mounted on shaft 2. The figures 5c/d display the time evolution and the spectral content of the applied torques. In the rest

of the paper, torques C_1 and C_2 will be refer as C.

6.4. Modal analysis

Table 2 displays the eigenfrequencies of the roots vacuum pump kinematic chain. The modal damping rate is set at 5% for each mode.

Mode number	Frequency (Hz)	Energy ρ_k (%)
1	0	0.0
2	173	0.0
3	174	0.0
4	618	0.9
5	664	0.0
6	679	0.0
7	731	0.0
8	733	0.0
9	780	2.3
10	871	0.0
43	11946	3.4
48	**15636**	**32.9**
52	16404	3.9
54	**17264**	**30.4**

Table 2: *Pump case: mesh modes energy*

On the one hand, low frequency modes may be excited by the low frequency components generated by the fluidic drag torque fluctuation (h4).
Mesh modes (see section 5, mainly the modes 48 and 54, may be excited by the mesh frequency components (h76, h152, h228...), as well as the components generated by the coupling between the drag torque fluctuation and the mesh stiffness fluctuation (h76 +/-h4, h152 +/-h4, h228 +/-h4...). The higher ρ_k is, the higher the d ynamic mesh force should be.

6.5. Amplitude spectrum of the dynamic mesh force

Figure 6 displays an example of the dynamic mesh force spectrum for the roots vacuum pump in the case of a standard operating regime $V = 4200$ rpm (70 Hz) and considering the square mesh stiffness fluctuation k_{sq}.

The dynamic mesh force is characterised by 4 different types of spectral components:

- The mean value h0 corresponds to the static mesh force induced by both STE and pumping drag torque mean values (see orange component in figure 6).
- The low frequency component h4 corresponds to the dynamic response to the pumping drag torque (in this example 280 Hz, corresponding to green component in figure 6).
- The high frequency components h76, h152, h228 and h304 correspond to the dynamic response to the STE fluctuations (in this example, respectively 4256 Hz, 8512 Hz, 12768 Hz and

17024 Hz, corresponding to pink components in figure 6). These high frequency components may also results from the coupling between the mesh stiffness fluctuations and both STE and pumping drag torque mean values.

- The lateral high frequency components h76 +/-h4, h152 +/-h4, h228 +/-h4 and h304 +/-h4 correspond to the dynamic coupling between the mesh stiffness fluctuations and the pumping drag torques fluctuations (in this example, 4032/4480 Hz, 8288/8736 Hz, 12544/12992 Hz and 16800/17248 Hz, corresponding to blue components in figure 6). This coupling results in a spectral enrichment of the dynamic response of the roots vacuum pump kinematic chain.

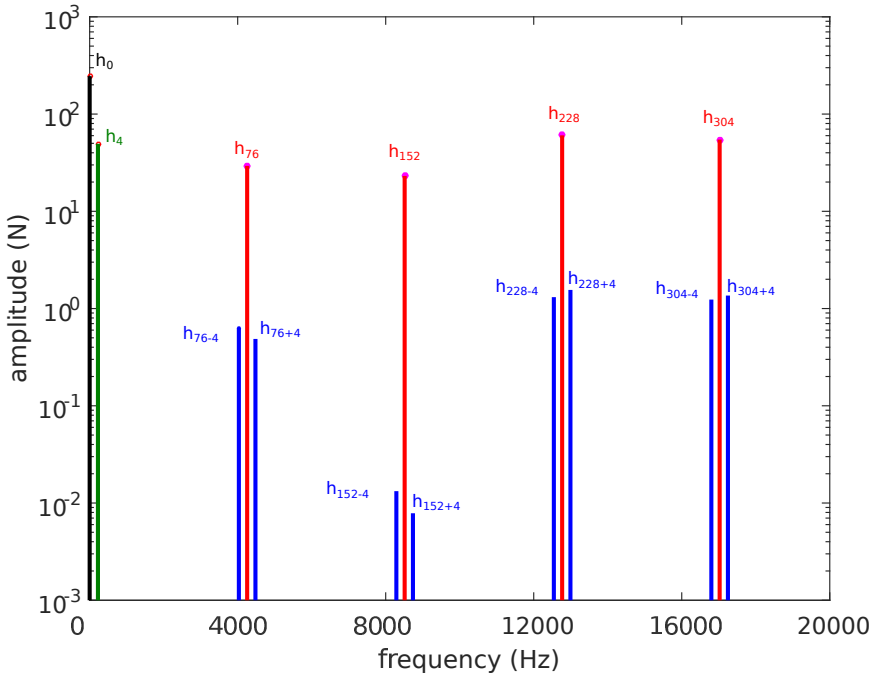

Figure 6: *Dynamic mesh force spectrum for a square mesh stiffness fluctuation and an operating frequency equal to 70 Hz (4200 rpm). Black components: mean value (h0). Green components: dynamic response to fluidic drag torque fluctuation $C(t)$ (h4). Red components: dynamic response to STE(t) and coupling between $k(t)$ and drag torque mean value (h76, h152, h228, etc...). Blue components: dynamic response to coupling between $k(t)$ and fluidic drag torque fluctuation $C(t)$ (h76 +/-h4, h152 +/-h4, h228 +/-h4, etc...)*

6.6. Dynamic mesh force: waterfall diagram and evolution of fluctuation RMS value versus operating rotation speed

Evolution of the dynamic mesh force versus operating regime is evaluated for the harmonic mesh stiffness fluctuation k_{sin} and the square mesh stiffness fluctuation k_{sq}. In order to ensure readability, simulations are carried out in 2 stages: first, STE fluctuation only is considered in addition to the mesh stiffness fluctuation. Second, pumping drag torque only is considered in addition to the mesh stiffness fluctuation.

Figure 7a,c,e,g display waterfall diagrams corresponding to the spectral content (in abscissa) and

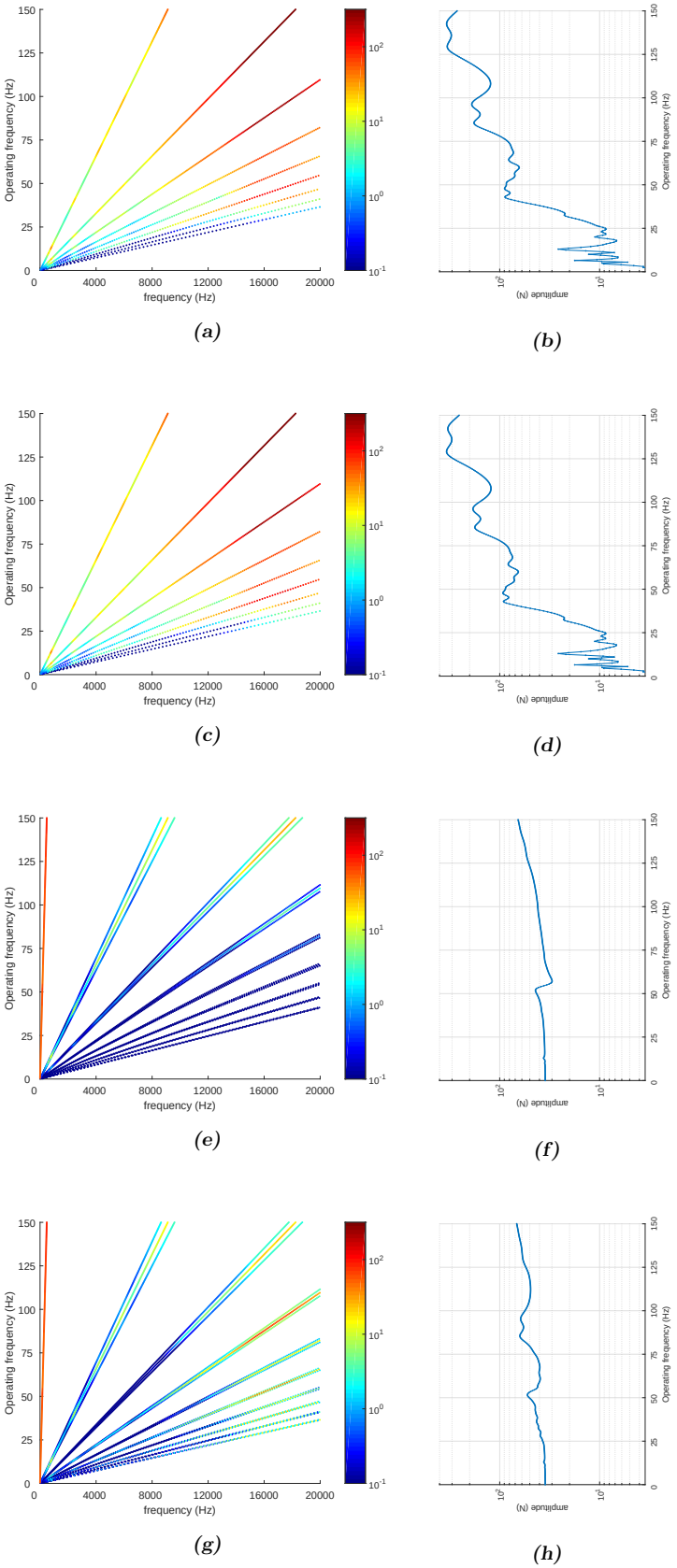

Figure 7: *Waterfall plots of the dynamic mesh force amplitude (N, colormap) and frequency content (Hz, in abscissa) versus operating frequency (Hz, in ordinate) for different excitation sources: (a) STE(t)+$k_{sin}(t)$, (c) STE(t)+$k_{sq}(t)$, (e) C(t)+$k_{sin}(t)$, (g) C(t)+$k_{sq}(t)$.*
Evolution of the dynamic mesh force fluctuations RMS value (N) versus operating frequency (Hz) for different excitation sources: (b) STE(t)+$k_{sin}(t)$, (d) STE(t)+$k_{sq}(t)$, (f) C(t)+$k_{sin}(t)$, (h) C(t)+$k_{sq}(t)$.

amplitude of the dynamic mesh force (color map) versus the roots vacuum pump operating rotation speed (in ordinate). Figures 7b,d,f,h display the corresponding evolution of the dynamic mesh force versus operating rotation speed.

- Figures 7a,b correspond to the harmonic mesh stiffness fluctuation k_{sin} and the STE(t) only.
- Figures 7c,d correspond to the square mesh stiffness fluctuation k_{sq} and the STE(t) only.
- Figures 7e,f correspond to the harmonic mesh stiffness fluctuation k_{sin} and the pumping drag torque only.
- Figures 7g,h correspond to the square mesh stiffness fluctuation k_{sq} and the pumping drag torque only.

Figures 7b,d show a large amplification of the dynamic mesh force due to the resonant excitation of the main mesh modes (15636 Hz, 32.9%) and (17264 Hz, 30.4%) by the successive harmonics of STE fluctuation. The most significant peaks are the following:

- For the operating frequencies $f = 85.5$ Hz and $f = 129$ Hz, the mesh mode 48 (15636 Hz, 32.9%) is excited by h228 ($f_{h228} = 15595$Hz) and h152 ($f_{h152} = 15686$ Hz).
- For the operating frequencies $f = 95.75$ Hz and $f = 142.5$ Hz, the mesh mode 54 (17264 Hz, 30.4%) is excited by h228 ($f_{h228} = 17465$ Hz) and h152 ($f_{h152} = 17328$ Hz).

Figures 7f,h show a slight amplification of the dynamic mesh force for the operating frequency $f = 52$ Hz, due to the resonant excitation of the low frequency modes 2 (173 Hz) and 3 (174 Hz) by the component h4 associated with the drag torque fluctuation. Figures 7f,h also show a slight amplification of the dynamic mesh force due to the resonant excitation of the main mesh modes (15636 Hz, 32.9%) and (17264 Hz, 30.4%) generated by the coupling between the mesh stiffness fluctuation drag torque (mean value h0 and fluctuation h4). The corresponding peaks are the following:

- For the operating frequencies $f = 85.5$ Hz and $f = 129$ Hz, the mesh mode 48 (15636 Hz, 32.9%) is excited by h228-h4/h228/h228+h4 and h152-h4/h152/h152+h4.
- For the operating frequencies $f = 95.75$ Hz and $f = 142.5$ Hz, the mesh mode 54 (17264 Hz, 30.4%) is excited by h228 h228-h4/h228/h228+h4 and h152-h4/h152/h152+h4. The resonant excitation of the mesh modes by the lateral components provides an enlargement of the amplification peaks of the dynamic response.

The waterfall diagrams 7e and 7g confirm that the coupling between the drag torque fluctuation and the mesh stiffness fluctuation induces some spectral components of the dynamic mesh force associated with harmonics of the mesh frequency and associated lateral components (h76, h76 +/- h4, h152, h152 +/-h4, etc.). The amplitude of the higher harmonics of the meshing frequency is not null, even if the stiffness fluctuation is purely sinusoidal. Nevertheless, the comparison of the diagrams shows that the amplitude of these components is much higher for a square mesh stiffness fluctuation, in particular for the odd harmonics (h76, h228, h380) associated with the spectral components of the square stiffness fluctuation.

Figure 8a,b display amplitudes of the dynamic mesh force (color map) versus the roots vacuum pump operating rotation speed (in ordinate) in the case of torque excitations, STE excitations, and

both excitations in the same simulation for the two mesh stiffness k_{sin} and k_{sq}. The comparison shows that the dynamic response of the kinematic chain is mainly generated by the drag torque fluctuation for operating regimes between 0 and 38 Hz. It is mainly generated by the STE fluctuation for operating regimes between 38 and 150 Hz.

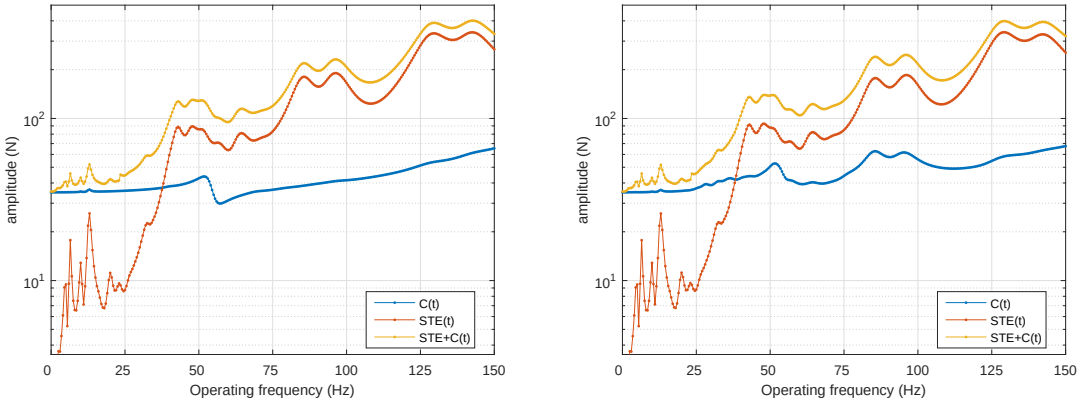

Figure 8: *Evolution of the dynamic mesh force fluctuation RMS value (N) versus operating frequency (Hz) for different excitation sources: (a) C(t)+STE+$k_{sin}(t)$, (b) C(t)+STE+$k_{sq}(t)$.*

7. Conclusion

This article presents a methodology for simulating vibro-acoustic response of mechanical geared systems. It corresponds to an extension of the previous spectral iterative method, with the introduction of terms resulting from the coupling between the parametric periodic stiffness associated with the gear mesh process and the external force fluctuation.
The procedure is based on the following principles:

- the dynamic response is projected onto the modal basis of the discretized system, computed from the mean values of mass and stiffness matrices,
- the N equations of the system are condensed into a single equation representing the dynamic transmission error,
- parametric equations of motion are solved in the spectral domain using an iterative schema, in order to obtain the dynamic response under steady-state operating conditions,
- dynamic response can be directly and easily extended to every degree-of-freedom of the discretized system.

The features of the procedure allow a fast computation compared to a classical time integration. The efficiency of the method is illustrated using a practical application corresponding to a roots vacuum pump. A finite element model of the kinematic chain is built in order to compute the modal basis. The mesh process generates high mesh frequency excitations corresponding to the static transmission error and the parametric mesh stiffness fluctuation. The pumping process generates a low frequency fluidic drag torque fluctuation. Both cases of sinusoidal and square mesh stiffness

fluctuations are considered. The coupling between mesh stiffness and drag torque fluctuations leads to a spectral enrichment of the dynamic response which is reflected on waterfall plots by emergence of numerous sidebands around harmonics of the mesh frequency. They induced not only an increase of the global fluctuation RMS value but they have also a significant impact on the nature of the dynamic response and the vibro-acoustic quality associated with the noise emitted from the roots vacuum pump. The richer the spectrum of the mesh stiffness is, the more significant the enrichment of the dynamic response and the impact on the vibro-acoustic quality of the mechanical system.

Acknowledgment

The authors are member of the LabCom LADAGE (LAboratoire de Dynamique des engrenAGEs), created by the LTDS and the Vibratec company and sponsored by the "Agence Nationale de la Recherche" in the program ANR-14-LAB6-0003. They are also member of the Labex CeLyA (Centre Acoustique Lyonnais). They would like to thank PFEIFFER VACUUM, VIBRATEC and INOPRO for their support in the context of the ARPE project (Acoustique et vibRation des Pompes à vidE, FUI AAP 19).

References

[1] D. Rémond, P. Velex, and J. Sabot. Comportement dynamique et acoustique des transmissions par engrenages: synthèse bibliographique (dynamic and acoustic analysis of gear transmissions: bibliographic reviews). Publication CETIM, 1993.

[2] D.B. Welbourn. Fundamental knowledge of gear noise: a survey. Technical report, 1979.

[3] S.L. Harris. Dynamic loads on the teeth of spur gears. Proceedings of the Institution of Mechanical Engineers, 172(1):87–112, 1958.

[4] E. Rigaud. Interactions dynamiques entre denture, lignes d'arbres, roulements et carter dans les transmissions par engrenages (Dynamic interactions between teeth, shaft lines, bearings, and housing in gear transmissions). PhD thesis, Ecole Centrale de Lyon, 1998.

[5] E. Rigaud and D. Barday. Modelling and analysis of static transmission error. effect of wheel body deformation and interactions between adjacent loaded teeth. In 4th world congress on gearing and power transmission, Paris, volume 3, pages 1961–1972, 1999.

[6] M.S. Tavakoli and D.R. Houser. Optimum profile modifications for the minimization of static transmission errors of spur gears. Journal of Mechanisms, Transmissions, and Automation in Design, 108(1):86–94, 1986.

[7] M. Umeyama. Effects of deviation of tooth surface errors of a helical gear pair on the transmission error. Nippon Kikai Gakkai Ronbunshu, C Hen/Transactions of the Japan Society of Mechanical Engineers, Part C, 61(587):3101–3107, 1995.

[8] S. Kurokawa, Y. Ariura, and M. Ohtahara. Transmission errors of cylindrical gears under load-influence of tooth profile modification and tooth deflection. American Society of Mechanical Engineers, Design Engineering Division (Publication) DE, 88:213–217, 1996.

[9] K. Umezawa, H. Houjoh, S. Matsumura, and S. Wang. Investigation of the dynamic behavior of a helical gear system: Dynamics of gear pairs with bias modification. In World congress on gearing and power transmission, pages 1981–1990, 1999.

[10] A Kahraman and G.W. Blankenship. Effect of involute tip relief on dynamic response of spur gear pairs. Journal of mechanical design, 121(2):313–315, 1999.

[11] A.L. Kapelevich and R.E. Kleiss. Direct gear design for spur and helical involute gears. Gear Technology, 19(5):29–35, 2002.

[12] C.H. Wink and A.L. Serpa. Investigation of tooth contact deviations from the plane of action and their effects on gear transmission error. Proceedings of the Institution of Mechanical Engineers, Part C: Journal of Mechanical Engineering Science, 219(5):501–509, 2005.

[13] A. Kahraman, P. Bajpai, and N.E. Anderson. Influence of tooth profile deviations on helical gear wear. Journal of Mechanical Design, 127(4):656–663, 2005.

[14] R. Guilbault, C. Gosselin, and L. Cloutier. Helical gears, effects of tooth deviations and tooth modifications on load sharing and fillet stresses. Journal of Mechanical Design, 128(2):444–456, 2006.

[15] G. Bonori, M. Barbieri, and F. Pellicano. Optimum profile modifications of spur gears by means of genetic algorithms. Journal of sound and vibration, 313(3):603–616, 2008.

[16] A. Carbonelli, J. Perret-Liaudet, E. Rigaud, and A. Le Bot. Particle swarm optimization as an efficient computational method in order to minimize vibrations of multimesh gears transmission. Advances in Acoustics and Vibration, 2011, 2011.

[17] L. Vedmar. On the design of external involute helical gears. na, 1981.

[18] E. Rigaud, J. Sabot, and J. Perret-Liaudet. Effect of gearbox design parameters on the vibratory response of its housing. In 4th World Congress on Gearing and Power Transmission, Paris, volume 3, pages 2143–2148, 1999.

[19] A. Carbonelli, E. Rigaud, and J. Perret-Liaudet. Vibro-acoustic analysis of geared systems - predicting and controlling the whining noise. In Automotive NVH Technology, pages 63–79. Springer, 2016.

[20] H.N. Özgüven and D.R. Houser. Dynamic analysis of high speed gears by using loaded static transmission error. Journal of Sound and Vibration, 125(1):71–83, 1988.

[21] D.R. Houser. Gear noise sources and their prediction using mathematical models. Gear Dynamics and Gear Noise Research Laboratory, Ohio State Univ., 1985.

[22] H. Vinayak, R. Singh, and C. Padmanabhan. Linear dynamic analysis of multi-mesh transmissions containing external, rigid gears. Journal of Sound and Vibration, 185(1):1–32, 1995.

[23] R.G. Munro. The dynamic behaviour of spur gears. PhD thesis, Cambridge University, 1962.

[24] M. Benton and A. Seireg. Simulation of resonances and instability conditions in pinion-gear systems. Journal of Mechanical Design, 100(1):26–32, 1978.

[25] J. Perret-Liaudet. Etude des mécanismes de transfert entre l'erreur de transmission et la réponse dynamique des boites de vitesses d'automobile (Study of tranfert mechanisms between static transmission error and dynamic response of automotive gearboxes). PhD thesis, 1992.

[26] Kazunori Ichimaru and Fujio Hirano. Dynamic behavior of heavy-loaded spur gears. Journal of Engineering for Industry, 96(2):373–381, 1974.

[27] S. Ohnuma, Y. Shigetaro, I. Mineicht, and T. Fujimoto. Sae paper 850979. Research on the idling rattle of manual transmission, 1985.

[28] R.J. Comparin and R. Singh. Non-linear frequency response characteristics of an impact pair. Journal of sound and vibration, 134(2):259–290, 1989.

[29] A. Kahraman and R. Singh. Non-linear dynamics of a spur gear pair. Journal of sound and vibration, 142(1):49–75, 1990.

[30] A. Kahraman and R. Singh. Interactions between time-varying mesh stiffness and clearance non-linearities in a geared system. Journal of Sound and Vibration, 146(1):135–156, 1991.

[31] G.W. Blankenship and A. Kahraman. Steady state forced response of a mechanical oscillator with combined parametric excitation and clearance type non-linearity. Journal of Sound and Vibration, 185(5):743–765, 1995.

[32] R.G. Parker, S.M. Vijayakar, and T. Imajo. Non-linear dynamic response of a spur gear pair: modelling and experimental comparisons. Journal of Sound and vibration, 237(3):435–455, 2000.

[33] S. Espin, J. Perret-Liaudet, and A. Kahraman. Étude théorique et expérimentale du comportement non-linéaire d'un engrenage droit induit par le jeu entre dents (theoretical and experimental study of non-linear spur gear behavior induced by gear backlash). Mécanique & Industries, 8(4):357–364, 2007.

[34] R. Singh, H. Xie, and R.J. Comparin. Analysis of automotive neutral grear rattle. Journal of sound and vibration, 131(2):177–196, 1989.

[35] A. Kahraman and R. Singh. Non-linear dynamics of a geared rotor-bearing system with multiple clearances. Journal of sound and vibration, 144(3):469–506, 1991.

[36] M. Barthod, J-L. Tébec, and M. Gizard. Etude du bruit dit de graillonnement dans les boıtes de vitesses automobiles (study of rattle noise in automotive gearbox). Mécanique & industries, 4(2):99–106, 2003.

[37] M. Barthod, B. Hayne, J-L. Tébec, and J-C. Pin. Experimental study of dynamic and noise produced by a gearing excited by a multi-harmonic excitation. Applied Acoustics, 68(9):982–1002, 2007.

[38] Y. Kadmiri. Analyse vibroacoustique du bruit de graillonnement des boîtes de vitesses automobiles (Vibroacoustic analysis of rattle noise in automotive gearbox). PhD thesis, Ecole Centrale de Lyon, 2011.

[39] Y. Kadmiri, E. Rigaud, J. Perret-Liaudet, and L. Vary. Experimental and numerical analysis of automotive gearbox rattle noise. Journal of Sound and Vibration, 331(13):3144–3157, 2012.

[40] F. Pfeiffer and W. Prestl. Hammering in diesel-engine driveline systems. Nonlinear Dynamics, 5(4):477–492, 1994.

[41] A. Kahraman and G.W. Blankenship. Interactions between commensurate parametric and forcing excitations in a system with clearance. Journal of Sound and Vibration, 194(3):317–336, 1996.

[42] A. Al-Shyyab and A. Kahraman. Non-linear dynamic analysis of a multi-mesh gear train using multi-term harmonic balance method: period-one motions. Journal of Sound and Vibration, 284(1):151–172, 2005.

[43] A. Al-Shyyab and A. Kahraman. Non-linear dynamic analysis of a multi-mesh gear train using multi-term harmonic balance method: sub-harmonic motions. Journal of Sound and Vibration, 279(1):417–451, 2005.

[44] P. Ziegler, P. Eberhard, and B. Schweizer. Simulation of impacts in geartrains using different approaches. Archive of Applied Mechanics, 76(9-10):537–548, 2006.

[45] J.S. Bendat. Principles and applications of random noise theory. Robert E. Krieger Pub. Co., 1977.

[46] N. Minorsky and T. Teichmann. Nonlinear oscillations. Physics Today, 15:63, 1962.

[47] C.S. Hsu and W-H. Cheng. Steady-state response of a dynamical system under combined parametric and forcing excitations. Journal of applied mechanics, 41(2):371–378, 1974.

[48] J. Perret-Liaudet. An original method for computing the response of a parametrically excited forced system. Journal of Sound and Vibration, 196(2):165–177, 1996.

[49] E. Rigaud, J. Sabot, and J. Perret-Liaudet. Comprehensive approach for the vibrational response analysis of a gearbox. Revue européenne des éléments finis, 1-3:315–330, 2000.

[50] A. Carbonelli. Caractérisation vibro-acoustique d'une cascade de distribution poids lourd (Vibroacoustic behaviour of a juggernaut multimesh gears transmission). PhD thesis, Ecole Centrale de Lyon, 2012.

[51] N. Driot, E. Rigaud, J. Sabot, and J. Perret-Liaudet. Allocation of gear tolerances to minimize gearbox noise variability. Acta Acustica united with Acustica, 87(1):67–76, 2001.

[52] Nicolas Driot and Joel Perret-Liaudet. Variability of modal behavior in terms of critical speeds of a gear pair due to manufacturing errors and shaft misalignments. Journal of Sound and Vibration, 292(3):824–843, 2006.

[53] L. Bachelet, N. Driot, G. Ferraris, and F. Poirion. Dynamical behavior of a rotor under rotational random base excitation. In ASME 2007 International Design Engineering Technical Conferences and Computers and Information in Engineering Conference, pages 1251–1260. American Society of Mechanical Engineers, 2007.

[54] L. Bachelet, N. Driot, and J. Perret-Liaudet. A spectral method for describing the response of a parametrically excited system under external random excitation. Journal of Computational and Nonlinear Dynamics, 3(1):011008, 2008.

[55] E. Rigaud and J. Sabot. Effect of elasticity of shafts, bearings, casing and couplings on the critical rotational speeds of a gearbox. VDI Berichte, 1230:833–845, 1996.